

Harmonic analysis in a large ring laser with backscatter-induced pulling

G. E. Stedman, Z. Li, C. H. Rowe, and A. D. McGregor

Department of Physics and Astronomy, University of Canterbury, Private Bag 4800, Christchurch, New Zealand

H. R. Bilger

School of Electrical and Computer Engineering, Oklahoma State University, Stillwater, Oklahoma 74078-0321

(Received 5 April 1994; revised manuscript received 12 December 1994)

Analytical solutions for the beam intensity, interferogram, and instantaneous phase are found for a ring laser with backscatter. The harmonics of these signals form geometric progressions, whose ratios depend differently on pumping, pulling, and the net backscatter phase. The latter phase depends on the time-reversal symmetry of the scatterers and on their location. We also report confirmatory results in the Canterbury ring laser system, with a quality factor up to 7.5×10^{10} and a present frequency resolution of 140 nHz, and where thermal changes in the net backscatter phase dominate other causes of drift.

PACS number(s): 42.60.-v

I. INTRODUCTION

The apparent Sagnac frequency detected in a ring laser is more generally the frequency difference derived from optical path nonreciprocity, whether this originates in rotation or not. In general, a time-reversal-violating mechanism is required. While the general proof of this was fully enunciated only recently [1], several partial anticipations may be noted in the literature [2–4]. However, time-even effects suffice to modify the nonreciprocal signal and the nominal frequency is pulled or pushed by a variety of effects. Another belated, if unconnected, realization of the importance of time-reversal considerations is introduced here in connection with the analysis of backscatter phases (Appendix A).

Locking phenomena in ring lasers have been studied extensively on account of their critical importance for the development of optical gyroscopes and the insight they give into laser dynamics [5–10]. When backscatter is present, numerical solutions of the laser equations have often been resorted to [8]. Recently experimental methods and theoretical results have given insights into the effects of pulling [11–16].

Etrich *et al.* [14] give a thorough study of possible solutions, both steady state (locked) and periodic (unlocked) as well as the domains of their stability, of the basic equations for the dynamics of a ring laser. In particular, they give an analytic solution to the intensity as well as the phase for the case of dissipative coupling, when the intensity variations of the two beams are approximately in phase, while the instantaneous frequency variations are antiphase. We extend such analytic solutions of the laser dynamics in the unlocked case so as to obtain analytic representations for the harmonic structure of the single beam intensities, the resultant interferogram, and the derived instantaneous phase in a ring laser gyroscope. The harmonic structure in the Fourier spectrum of the interferometer signal in a ring laser was observed in our laser system [17–19], which has an area of 0.7547 m^2 , a quality

factor $Q \sim 7.5 \times 10^{10}$, a finesse $F \sim 1.4 \times 10^4$, and has already attained a frequency precision at the microhertz level [1]. Here we find answers to the questions that were implicitly raised by this earlier work.

In particular, we establish the theoretical interpretation of the harmonic structure in each of the single beam signals, the interferogram, and the instantaneous phase [17,18]. In the first two cases these are combination effects of laser gain and of frequency pulling. Within approximations we derive the characteristic Airy profile in the time domain and the related geometric progression in the frequency domain for all of these spectra. For the dissipative case at least, the harmonics of the single beam intensity, the interferogram, and the instantaneous phase form geometric progressions, but the ratios depend in different ways on the various parameters. A simple physical interpretation is given in Appendix B. Observations of the time and frequency domain structure of all these spectra are reported here and are in agreement with these predictions. When the lock-in threshold is of similar size to the bias frequency in a ring laser, the pulled frequency can be measured by monitoring the intensity of a single beam. The overall phase of the backscatter affects both amplitude and phase variations in either beam. The temporal intensity variations in each beam furnish a significant component of the spectral behavior of the interferogram. The anharmonic effects of intensity and phase variations tend to cancel both in the single beam intensity and in the interferogram. In principle, the time dependence and harmonic content of the interferometrically derived beat signal, of each beam intensity, and of the instantaneous frequency derived from these give complementary information.

In the more complicated special cases we restrict ourselves to the standard extremes of conservative (or Hermitian) coupling and of dissipative coupling [5,14,11] when the net backscatter phases ϵ_+, ϵ_- for the two counter-rotating beams have a sum $2\zeta = \pi, 0$, respectively. We prove, by an extension of the argument of

Haus *et al.* [5], that the intrinsic distinction between conservative and dissipative coupling at each scatterer reflects the symmetry or antisymmetry of the physics of the scattering process under time reversal (Appendix A). However, as Christian and Mandel [13] and Rodloff [20] showed, the transmutation between these two forms of coupling, in particular the sum of the net backscatter phases, depends not only on such fundamental symmetries of the scattering centers but also, and critically, on the distances between the scattering centers and the beam combiner. One consequence is that the lock-in threshold and so the observed frequency pulling are functions of temperature-induced changes in cavity length. In our laser system, where rf excitation reduces Langmuir effects, etc., this turns out to be the dominant form of Sagnac frequency drift. Understanding the origins of this drift is our second major practical reason for the present investigation.

A third reason is that the present study is an essential prerequisite for a determination of the effects of laser gain and frequency pulling on the magnitudes and separations of sidebands generated on the Sagnac spectral line and on its harmonics by both periodic and aperiodic variations in the rotation rate, such as the seismic effects we study elsewhere [21], and ultimately in a fuller geophysical analysis [19,22].

Finally, in both this and the present connection we document here the numerical analytical methods, which allow us to dedrift experimental results numerically. This is an essential step both in achieving the microhertz level of frequency discrimination reported before [1] and in constructing the instantaneous phase and frequency whose spectra are studied here.

II. PERIODIC SOLUTIONS WITH BACKSCATTER

A. General

We take as our reference point A of the ring the position of the output mirror leading to the beam combiner. Let each beam \pm , where $+$ denotes counterclockwise (CCW) and $-$ clockwise (CW), have a complex amplitude given by a phasor $\tilde{E}_{\pm} = E_{\pm} \exp i\phi_{\pm}$. Its phase $\phi_{\pm} = \omega_{\pm}(t - z_{\pm}/c)$; ω_{\pm} are the corresponding actual mode frequencies (including corrections for dispersion, etc.) and z_{\pm} (z_{-}) is the optical path length around the ring from A in a CCW (CW) sense. We take P_{\pm} as the total optical path lengths, so that $\omega_{\pm}P_{\pm} = 2\pi cN$. The nonreciprocity in frequency (derived from optical path nonreciprocity and ultimately from time-reversal violation) is $f = (\omega_{+} - \omega_{-})/2\pi$.

Each of the complex time-dependent phasors \tilde{E}_{\pm} for the CCW and CW beams at A changes in unit time for several reasons, which are discussed in detail in earlier papers. First, there is the natural time dependence given by the $\omega_{\pm}t$ part of ϕ_{\pm} ; this may be expressed by writing $d\tilde{E}_{\pm}/dt = i\omega_{\pm}\tilde{E}_{\pm}$. Second, laser pumping, saturation, and cross saturation (parametrized by a, β, ξ ,

respectively) will scale the amplitude of the phasor \tilde{E}_{\pm} by a factor, per unit time, of $\pi a - \beta E_{\pm}^2 - \xi E_{\mp}^2$. Third, as the result of a backscattering rate of $R_{\mp}\tilde{E}_{\mp}$ into each of the \pm beams from the other beam, $d\tilde{E}_{\pm}/dt = R_{\mp}\tilde{E}_{\mp}$ (where we define amplitudes and phases of these complex backscattering coefficients R_{\mp} by $R_{\mp} = r_{\mp} \exp i\epsilon_{\mp}$; see Appendix A). In total,

$$\frac{d\tilde{E}_{\pm}}{dt} = (i\omega_{\pm} + \pi a - \beta E_{\pm}^2 - \xi E_{\mp}^2) \tilde{E}_{\pm} + R_{\mp} \tilde{E}_{\mp} \exp i\epsilon_{\mp}. \quad (1)$$

Together these terms cover the key physical features of laser dynamics included in earlier analyses [8,11,13,14,20]. We deduce the following differential equations for the phasors' real amplitudes $E_{\pm}(t)$ and phases $\phi_{\pm}(t)$:

$$\frac{1}{E_{\pm}} \frac{dE_{\pm}}{dt} = (\pi a - \beta E_{\pm}^2 - \xi E_{\mp}^2) + \rho_{\mp} \cos(\psi \mp \zeta), \quad (2)$$

$$\frac{d\phi_{\pm}}{dt} = \omega_{\pm} \mp \rho_{\mp} \sin(\psi \mp \zeta), \quad (3)$$

where the beam-amplitude-scaled backscatter parameters $\rho_{\pm} \equiv r_{\pm} E_{\pm}/E_{\mp}$, the relative beam phase $\psi \equiv \phi_{+} - \phi_{-} + (\epsilon_{+} - \epsilon_{-})/2$, and the net backscatter phase $\zeta \equiv (\epsilon_{+} + \epsilon_{-})/2$. The differential equation for ψ is

$$\frac{d\psi}{dt} = 2\pi f - \rho_{-} \sin(\psi - \zeta) - \rho_{+} \sin(\psi + \zeta). \quad (4)$$

If for the moment we suppose that $\rho_{+} = \rho_{-} \equiv \rho$, we can write

$$\frac{1}{2\pi} \frac{d\psi}{dt} = f - l_{\zeta} \sin \psi, \quad l_{\zeta} \equiv \frac{\rho}{\pi} \cos \zeta. \quad (5)$$

When (the conservative case) $\zeta = \pi/2 \bmod \pi$, then $l_{\zeta} = 0$ and backscattering affects the phase of the two phasors \tilde{E}_{\pm} equally and does not affect the relative phase ψ whose measurement is of interest for gyro purposes. This is equivalent to the condition that the two backscatter parameters obey the equation [13] $R_{+} + R_{-}^{*} = 0$ in this limit.

When (the dissipative case) $\zeta = 0 \bmod \pi$, then $l \equiv l_0$ and is maximal and the phase changes of the phasors are opposite, maximally affecting ψ .

However, the ρ_{\pm} are not constants; the effect on the intensities in every case has a similar significance to that of the backscattering phenomenon itself. As shown by Eq. (2), the backscattering rates r_{\pm} directly affect the time variations of the magnitudes of the intensities. For small variations, both intensities are simple sinusoidal functions of the pulled phase and Eq. (2) shows directly that, as far as the trigonometric factor in the backscattering is concerned, the phase difference between these beam intensity variations is itself 2ζ . Hence in the dissipative (conservative) case, the beam intensity variations are in phase (antiphase, respectively). The pivotal role of the net backscatter phase ζ has been recognized by Haus *et al.* [5] Christian and Mandel [12,13], and Wilkinson [11]

for example. We shall assume the equality only of the magnitudes $r_+ = r_- \equiv r$ of the fractional backscattering coefficients in the following. This is consistent with time-reversal invariance of each scatterer (see Appendix B) and makes an analytic calculation feasible, but is less severe than the assumption that the beam-amplitude-scaled backscatter coefficients ρ_{\pm} are constants.

B. Dissipative case

In the dissipative limit ($\zeta = 0$), Eq. (2) takes the form:

$$\frac{1}{E_{\pm}} \frac{dE_{\pm}}{dt} = (\pi a - \beta E_{\pm}^2 - \xi E_{\mp}^2) + \rho_{\mp} \cos \psi, \quad (6)$$

$$\frac{d\psi}{dt} = 2\pi f - r \frac{E_+^2 + E_-^2}{E_+ E_-} \sin \psi. \quad (7)$$

Let us define the symmetric (E) and the antisymmetric (A) parts of the beam intensities by

$$E = \frac{1}{2}(E_+^2 + E_-^2), \quad A = \frac{1}{2}(E_+^2 - E_-^2). \quad (8)$$

From Eqs. (6) and (8),

$$\frac{1}{2E} \frac{dE}{dt} = \pi a - 2\beta E + \frac{1}{E}[(\beta - \xi)(E^2 - A^2) + r\sqrt{E^2 - A^2} \cos \psi], \quad (9)$$

$$\frac{1}{2A} \frac{dA}{dt} = \pi a - 2\beta E. \quad (10)$$

If the net gain (pumping as reduced by saturation and cross relaxation) is sufficiently small to have less effect on these beam intensities than backscattering, $|\pi a - (\beta + \xi)E| \ll r$. In our case, this is reasonable since we operate our He-Ne laser in monomode with total pumping powers of a few watts and exit powers of the order of nanowatts. For mathematical convenience we make the somewhat stronger assumption that $|\pi a - 2\beta E| \ll |(\beta - \xi)E + r|$; this is certainly true if backscatter is more important than net gain and also than the difference between saturation and cross relaxation. In this case pulling dominates the beam dynamics and from Eq. (10) $A = 0$, i.e., the intensities of the two beams are equal: $E_+ = E_-$. The above makes explicit the approximation made by Etrich *et al.* [14], who merely assumed this equality. This uncouples Eq. (7) from Eq. (6), giving the Adler-type equation

$$\frac{1}{2\pi} \frac{d\psi}{dt} = f - l \sin \psi, \quad (11)$$

where [as in the appropriate limit of Eq. (5)] $l = r/\pi$. This has the solution

$$\psi(t) = 2 \arctan \frac{v}{f} = 2 \arctan \frac{\sin(\pi p t + \chi)}{\cos \pi p t}, \quad (12)$$

where

$$v \equiv l + p \tan \pi p t, \quad \chi \equiv \tan^{-1} \left(\frac{l}{p} \right), \quad p \equiv \sqrt{f^2 - l^2},$$

p being the pulled frequency. An alternative method for deriving ψ will be given in connection with the analytic signal approach in Sec. III. Further details concerning this and later derivations are given in Appendix C.

The observed instantaneous frequency, corresponding to that recovered from the analytic signal, is then, from Eqs. (11) and (C2):

$$f_0 = \frac{1}{2\pi} \frac{d\psi}{dt} = \frac{p^2}{f - l \cos 2\pi p t} = (f + l) \frac{1 + \tan^2 \pi p t}{1 + u \tan^2 \pi p t}, \quad (13)$$

where the ratio $u \equiv (f + l)/(f - l)$. The period of the frequency excursions $T = 1/p$.

From Eq. (13), the observed frequency varies between $f + l$ and $f - l$. However, it is not symmetrical in between so that its average value, or pulled frequency f_0 — that determined from gyro output counts — is not f but p . Appendix C gives one proof, which leads to the material below.

Fourier analysis of the instantaneous frequency gives a geometric progression of harmonics (Appendix C) whose ratio r is given by

$$r = \left(\frac{f - p}{l} \right). \quad (14)$$

This may be written as $r = R(q)$, where

$$R(q) \equiv q - \sqrt{q^2 - 1} \quad (15)$$

and $q = f/l$. Note that $R(q)$ is a monotonically decreasing function of q . In the limit $q \rightarrow \infty$, $R(q) \rightarrow 1/2q$. Hence, in the above application with $q = f/l$, for progressively lower lock-in thresholds, $r \rightarrow 0$ linearly with l : $R(f/l) \rightarrow l/2f$. Hence harmonics (as opposed to the fundamental signal) of the instantaneous frequency exist only because of the existence of backscatter, pulling, and a lock-in threshold. The instantaneous phase [Eq. (12)] will have a harmonic structure that is altered from this geometric progression by a factor $1/n$ generated by the $1/\omega$ factor arising in the integration.

Further manipulation (Appendix C) shows that this allows the representation

$$\psi = \arg \left(\frac{1}{1 - r \exp 2\pi i p t} \right) = \arg Z, \quad (16)$$

where Z is the analytic signal whose real part corresponds to the Fourier expansion of Eq. (C7). The analytic signal then has the form familiar from Fabry-Pérot theory

$$Z(t) = C' \sum_{n=0}^{\infty} (r \exp 2\pi i p t)^n = \frac{C}{1 - r \exp 2\pi i p t}; \quad (17)$$

its modulus is the Airy function. This is reflected experimentally in the temporal form of the interferometer signal $X(t)$ (discussed later on in this section), which resembles an Airy function; the more nearly the ratio r approaches unity, the more sharp are its features. This same general behavior is found whenever the harmonics of a signal are in geometric progression.

For intensities, and with $A = 0$, Eq. (9) becomes

$$\frac{1}{2E} \frac{dE}{dt} = \pi a - bE + \pi l \cos \psi, \quad (18)$$

where the nonlinear coupling parameter $b \equiv \beta + \xi$. This may be solved analytically, through a generalization of the work of Etrich *et al.* [14] (Appendix C), so that

$$E = \left(\frac{\pi a}{b} \right) \frac{h^2 (f + l \sin 2\theta)}{h^2 f + h a l \sin (2\pi p t + \gamma) - l p K \exp(-2\pi a t)}, \quad (19)$$

where the shifted phase $\theta \equiv \pi p t + \chi/2$ (Appendix C) and the parameter $h \equiv \sqrt{a^2 + p^2}$, corresponding to a combination of pumping and pulling, and a shifted phase $\gamma \equiv \chi - \arctan p/a$.

Hence the associated time dependence of the beam intensities is as nontrivial as that of the instantaneous frequency [Eq. 13] and in particular shares the same frequency p . Note also that the limiting case $l \rightarrow 0$, to which we now restrict ourselves, gives the obvious solution of the differential equation: $E \rightarrow \pi a/b$. The denominator on its own gives a geometric progression of harmonics, now with the ratio [compare Eq. (15)]

$$r_I = R \left(\frac{h f}{a l} \right). \quad (20)$$

Since pulling is present and so $h > a$, the argument $h f/a l$ of R is greater in the case of the single beam variations [Eq. (20)] than for the corresponding value f/l for the instantaneous frequency [Eq. (13)]. Hence the corresponding ratios are in the opposite order, since R is a monotonically decreasing function. This has the paradoxical consequence that despite the absence of the harmonic effects of beam intensity variations, the harmonic structure of the instantaneous frequency is richer than that of the single beam spectra. Hence the function R itself is less and the variations in the instantaneous single-beam intensities are more nearly harmonic than those in the instantaneous frequency. Comparing their relative anharmonicity gives information about h/a and so gives the gain parameter a directly in units of the (observed) pulled frequency p . In this sense the effects of beam intensity variations and backscatter tend to cancel. An extension of this is given in Appendix C.

The observed signal is the result of beating together the two individual beams, we assume in equal proportions: the intensities are the same (time-dependent) value E and the phases differ by ψ . This gives an intensity for the interferometric pattern proportional to

$$X(t) = |\sqrt{E} + \sqrt{E} e^{i\psi}|^2 = E(1 + \cos \psi). \quad (21)$$

As a result the full interferometer signal—incorporating the time dependence of both the intensity and phase—has the form in which two major time-dependent terms, one in the intensity factor [Eq. (19)] and one in the phase factor [Eq. (C2)], have canceled:

$$X = \left(\frac{\pi a}{b} \right) \frac{h f (1 + \cos 2\pi p t)}{h f + a l \sin (2\pi p t + \gamma)}. \quad (22)$$

The resulting interferometer wave form [Eq. (22)] has a time dependence that is similar to that of the single beams [Eq. (19)] (Appendix C).

In principle, any experimental interferogram record $X(t)$ could yield each ratio on analysis (the instantaneous frequency being derivable from the corresponding analytic signal) and (since a, p are derived parameters) each of the parameters a, l could then be inferred from a knowledge of f, r, r_I . The detailed wave form from the interferometer is thus a diagnostic of the state of the ring laser.

C. Conservative case

In the conservative case ($\zeta = \pi/2$), Eqs. (2) and (4) become

$$\frac{dE_{\pm}}{dt} = (\pi a - \beta E_{\pm}^2 - \xi E_{\mp}^2) E_{\pm} \pm r E_{\mp} \cos \psi, \quad (23)$$

$$\frac{1}{2\pi} \frac{d\psi}{dt} = f + r \left(\frac{E_+^2 - E_-^2}{2\pi E_+ E_-} \right) \sin \psi. \quad (24)$$

From Eqs. (23) and (8),

$$\frac{1}{2E} \frac{dE}{dt} = \pi a - 2\beta E + \frac{1}{E} (\beta - \xi) (E^2 - A^2), \quad (25)$$

$$\frac{1}{2A} \frac{dA}{dt} = \pi a - 2\beta E + \frac{r}{A} \sqrt{E^2 - A^2} \cos \psi. \quad (26)$$

Assumptions similar to our previous ones: $|\pi a - 2\beta E| \ll r$, $|(\beta - \xi) \sqrt{E^2 - A^2}| \ll r$, ensure again that pulling dominates the beam dynamics. From Eq. (26) $dE/dt = 0$, i.e., E is a constant (which we denote E_0 for clarity) and the intensities of the two beams fluctuate in antiphase [11]. Also

$$\frac{1}{2\pi} \frac{d\psi}{dt} = f + \frac{l A}{\sqrt{E_0^2 - A^2}} \sin \psi. \quad (27)$$

Using the definition $A = E_0 \sin \alpha$,

$$\frac{1}{2\pi} \frac{d\alpha}{dt} = l \cos \psi, \quad \frac{1}{2\pi} \frac{d\psi}{dt} = f + l \tan \alpha \sin \psi. \quad (28)$$

This shows that in the conservative case, and when intensity variations in time are allowed for, phase variations (nonlinear variations in time corresponding to spectral components at a pulled frequency) can exist as for a changed (reduced), but nonzero, value of lock-in threshold in Eq. (28) since the lock-in threshold l of Eq. (11) is replaced by $l \tan \alpha$.

Analytic solutions of this equation are possible under further approximation. If the locking effects are small, α may be taken to be approximately a constant $\bar{\alpha}$ in the phase equation. We retrieve the Adler type of solution, in which the lock-in threshold is reduced by a factor $\tan \bar{\alpha}$:

$$\psi(t) - \pi = 2 \arctan \frac{w}{f} = 2 \arctan \frac{\sin(\pi q' t + \sigma)}{\cos \pi q' t}, \quad (29)$$

where $m = l \tan \bar{\alpha}$, $q' = \sqrt{f^2 - m^2}$, $w = m + q' \tan \pi q' t$, $\sigma = \tan^{-1}(m/q')$, and $k = \sqrt{q'^2 + a^2}$. The harmonic content of the instantaneous frequency is therefore a geometrical progression as for the dissipative case, with a ratio $r_C = R(f/m)$.

If we then insert this phase solution in the intensity equation, we find the first-order changes in intensity that result:

$$\alpha = 2\pi l \int dt \cos \psi = \frac{l}{m} \ln [f + m \sin(2\pi q' t + \sigma)]. \quad (30)$$

Equation (30) describes the harmonic structure of the antiphase variations in the beam intensity for small pulling. Again these variations are seen to be commensurate with those in the phase itself.

The interferometric pattern is now proportional to

$$X(t) = |E_- + E_+ e^{i\psi}|^2 = 2E_0 (1 + \cos \alpha \cos \psi). \quad (31)$$

Hence its time dependence will be the product of that in $\cos \alpha$ [see Eq. (30)] and $\cos \psi$ [Eq. (29)] separately. The Fourier spectrum will then be the convolution $\mathcal{X} = \mathcal{A} \otimes \Psi$ of the geometric progression associated with the Fourier transform Ψ of $\cos \psi$ ($\Psi = \mathcal{F}[\cos \psi]$) and the Fourier transform $\mathcal{A} = \mathcal{F}[\cos \alpha]$ of the intensity-dependent factor. The effect on the beat signal and its Fourier analysis of the intensity variation is thus seen to be non-negligible and to be enshrined in $\mathcal{F}[\cos \alpha]$, whose analytic solution is not available. In the limit in which we take α to be approximately constant, Eq. (31) reduces to the general form of Eqs. (19) and (21) and similar comments are applicable; in particular, we expect a geometric progression of harmonics with the ratio

$$r_D = R\left(\frac{kf}{am}\right) \quad (32)$$

for small lock in.

D. General backscatter phase

We shall need also solutions for the case of general ζ , which also will be illustrated from experiment in Sec. IV B. For these to be analytic, we concentrate on the effects of pulling and assume that backscatter dominates the beam dynamics, setting $a = \beta = \xi = 0$. The single beam intensity variations given through Eq. (2), when rewritten in this limit, take the form

$$\frac{1}{E_{\pm}} \frac{dE_{\pm}}{dt} = \rho \cos(\psi \mp \zeta). \quad (33)$$

We also revert to the assumption, valid in the case of relatively weak backscatter, that intensity variation is unimportant for the phase dynamics, so that from Eq. (5)

$$\frac{1}{2\pi} \frac{d\psi}{dt} = f - l \sin \psi, \quad (34)$$

where in this subsection only we write l for $l_{\zeta} \equiv$

$(\rho/\pi) \cos \zeta$, assumed to be a constant in time, and similarly for the derived quantities p, v, χ, θ (for example, $p = p_{\zeta} \equiv \sqrt{f^2 - l_{\zeta}^2}$). It follows that the solution for the instantaneous phase ψ and the derived quantities such as the instantaneous frequency, and the analytic signal and interferogram so far as they are not greatly affected by intensity fluctuations, have the same algebraic form as for dissipative coupling and in particular a geometric progression of harmonics, with the ratio $r_G = R(f/l)$. To be precise, Eq. (34) has the solution of Eq. (C2) as modified by these redefinitions:

$$\cos \psi = \frac{f^2 - v^2}{f^2 + v^2} = \frac{p \cos 2\theta}{f + l \sin 2\theta}. \quad (35)$$

Hence Eq. (33) takes the form

$$\frac{d \ln E_{\pm}}{dt} = \rho \left(\frac{p \cos 2\theta \cos \zeta \pm (l + f \sin 2\theta) \sin \zeta}{f + l \sin 2\theta} \right). \quad (36)$$

This has the solution

$$\begin{aligned} \frac{2pl\pi}{\rho} \ln E_{\pm} = & p \cos \zeta \ln (f + l \sin 2\theta) \\ & \pm 2 \sin \zeta \left(f \arctan (\tan \theta) \right. \\ & \left. - p \arctan \frac{l + f \tan \theta}{p} \right) + C, \end{aligned} \quad (37)$$

where C is a constant. The dissipative and conservative limits of these equations show as before that the individual beams are respectively in phase and antiphase; the first term on the right-hand side of Eq. (37) has the same form for each beam and controls the dissipative case, whereas the second and third terms in large parentheses define the beam intensity variations, with opposite signs for the two beams, in the conservative case. Hence the beam intensities can be written as a product of the exponentials of the three terms on the right-hand side of Eq. (37) and the harmonic structures of each, including the $(1/\omega)$ -weighted geometric progression arising from the last term, are convolved in the Fourier domain.

Further comments on the general case are given in Appendix C.

III. ANALYTIC SIGNAL PROCESSING OF INTERFEROGRAMS

The standard method of isolating the phase information is to count zero crossings of the interferogram. An alternative technique proposed and illustrated in this paper is to use the full interferometric wave form to construct the analytic signal, so recovering pure phase information. We describe one possible approach in the context of the signal processing package MATLAB. In the procedure HILBERT, the real signal $X(t)$ is converted to the analytic signal $Z(t) = X(t) + iY(t)$, where $Y(t)$ is the Hilbert transform

$$Y(t) = \frac{1}{\pi} \int dt' \frac{X(t')}{t-t'}. \quad (39)$$

This is achieved most simply by noting that $Z(\omega) = \mathcal{F}(Z(t))$, the Fourier transform of $Z(t)$, differs from $\mathcal{X}(\omega)$ principally by having all negative frequency components set to zero in the latter; what is a cosine in the real part is a sine in the Hilbert transform and their negative frequency parts have opposite sign and cancel on forming the analytic signal [23,24]. This gives a minimum-phase estimate of the analytic signal, as is appropriate for a passive and causal physical system. The instantaneous phase $\Phi(t) = \arg(Z(t))$ may then be derived by using the procedure UNWRAP on the principal-value phase—a process for which the MATLAB 4.2 routine is unreliable in our application; we find it best to rewrite it assuming a monotonic behavior of $\Phi(t)$. The resulting phase is expected to correspond to the instantaneous phase derived from a technique such as zero crossing, in the appropriate limits to accord with the results of Eqs. (12) and (29). We have proved in Sec. II B and in a variety of circumstances that signals whose harmonics form a geometric progression have an important role and that when this is so, the instantaneous phase ψ has the same harmonic structure whether it is derived from the analytic signal or from the associated differential equation.

Hence the relationship between the Fourier components of the instantaneous phase associated with any signal contains no new information in principle. In practice, however, it can furnish an independent experimental approach for confirmation of the applicability of the model.

In practice the drifts associated (as we find) with thermally induced variations in pulling need to be removed. The standard experimental procedures of using a servo system to piezocontrol the path length are inadequate and in any case difficult for us. We prefer a numerical dedrifting procedure after the experimental run has been made. This is reliably achieved by the following method (referred to by the MATLAB procedural name GPROC). For long runs, we use a heavily aliased signal $V(t)$, typically with 1–2 samples per second, and dealias at the end by hand comparison with a plot of the running fast Fourier transform (FFT). We coarsely frequency filter the interferometer spectrum $\mathcal{V}(\omega) = \mathcal{F}(V(t))$ so as to concentrate on the region of interest, usually near the Sagnac Earth rotation line ($\simeq 69$ Hz). The corresponding analytic signal $Z(t) = \mathcal{F}^{-1}(\mathcal{V}(\omega), \omega > 0)$ has a phase $\Phi(t)$ whose frequency spectrum $\mathcal{P}(\omega)$ itself contains both the low-frequency $\Phi_d(t)$ drifts we wish to eliminate — below a cutoff frequency f_{cut} of say 0.0005 Hz, this threshold corresponding to the time constant chosen in any hard-wired phase sensitive detection process — and the information of interest $\Phi_\beta(t)$ (say 50–90 Hz). We high-pass filter $\mathcal{P}(\omega) \rightarrow \mathcal{P}_f(\omega)$ by removing the lowest components in all bins up to the cutoff frequency f_{cut} . Typically only a few hundred bins in a total of a few hundred thousand are so affected; in other words, $f_{\text{cut}} \ll f_N$, the Nyquist frequency. We then form the corresponding spectrum $\mathcal{V}_f(\omega) = \mathcal{F}(\text{Re}[|Z(t)| \exp i\mathcal{F}^{-1}(\mathcal{P}_f(\omega))])$. This is the algorithm used in Sec. IV B. Arguably one would get

cleaner and more impressive results by leaving out $|Z(t)|$ and its associated noise in this restoration; however, we have retained it in all results reported so far so as to display all sources of the relatively high frequency noise in the signal, apart from the low-frequency drift term $\Phi_d(t)$. Clearly one can track almost any carrier as closely as desired and so reduce its real frequency noise apparently to zero by taking a sufficiently high cutoff frequency f_{cut} , just as one can in principle electronically lock as close as desired to a drifting line by choosing an appropriate time constant for the electronic servo loop. On the other hand, smaller bandwidths reduce other noise. The important consideration here in both the electronic and the numerical case is the choice of cutoff frequency; all amplitude noise, and all frequency noise in the range f_{cut} to f_N are retained and their effects displayed. We always choose $f_{\text{cut}} \ll f_N$ and so retain in principle all amplitude noise information and nearly all frequency noise information in a frequency band of width f_N . If the laser drift is substantial, we find that our procedure does not lock onto the carrier when the cutoff is chosen to be as low as $f_{\text{cut}} \sim 0.0005$ Hz. Nevertheless, this method on better data used with such cutoffs locks and then yields the remarkably narrow Sagnac frequency line previously reported [19,1]. A subsequent run 96AG26 has yielded an even narrower line (see Sec. IV B).

A defect of this method is that it is not possible to preserve fully the sideband structure of the line that is being locked. This, with a more satisfactory alternative for sideband analysis, will be discussed elsewhere [21] in the context of seismic studies.

IV. EXPERIMENT

A. Canterbury ring laser

There has been renewed interest recently in the possibility of a significant step forward in ring laser technology to “supergyroscopes,” larger than have heretofore been considered practical [25,19]. Drifts associated with frequency pulling remain a major limitation on the performance of such devices.

Our He-Ne ring laser system [17–19] is defined by a rectangle of four supermirrors, nominally 99.9985% reflectors, and having measured total losses at manufacturing in the range 8–14 ppm, of which up to 10 ppm constitute the (designed) transmission loss and 3–5 ppm are measured as scattering loss. The mirrors are mounted in superinvar mounts and are placed directly on a 1.2 m \times 1.2 m \times 25 mm Zerodur plate, itself mounted on a 700 kg granite block. Stainless steel boxes, which are sealed by Viton O rings on the Zerodur, surround but do not touch these mirrors and the connecting Pyrex tubes (i.d. 10 mm) do not intersect the beam, which is always within the lasing gas. Part of this tube is a narrower fused silica tube (i.d. 4 mm, length 200 mm) with a cylindrical radio frequency exciter surrounding it. Since the beam never intersects a solid surface, maximal quality factors become feasible. The laser has an effective area of 0.7547 m² (as determined from the longitudinal mode frequency spacing and the measured dimensions) and a (recently re-

measured) quality factor $Q = 7.5 \times 10^{10}$. Alignment of the mirrors can be done only in open air with the cover plates removed and prior to pumpdown. To assist, we recently installed a basic clean air system (an Enviroco Corp. Hospi-Gard system, with throughput $14 \text{ m}^3/\text{min}$ and 99.97% retention of particles $> 0.3 \mu\text{m}$). The ring laser is operated in monomode with a radio frequency pump power of the order of a few watts, a circulating power of the order of milliwatts, and an exit beam power of the order of nanowatts. If we take the sidereal day to be 23 h, 56 m, the Earth's rotation has an angular velocity Ω of magnitude $7.292 \times 10^{-5} \text{ rad/s}$. Its Sagnac effect generates a spectral line (which we call for brevity the Earth line) in the Fourier transform of the interferometer signal whose (beat) frequency is nominally

$$f_b = 4\mathbf{A} \cdot \boldsymbol{\Omega} / \lambda P. \quad (40)$$

In this equation, the perimeter P is determined from radio frequency measurements of the free spectral range as $3.47710 \pm 0.00010 \text{ m}$, the He-Ne laser wavelength $\lambda = 633.0 \text{ nm}$, and the corresponding frequency f_0 is 473.6 THz ; hence, at our latitude Λ of $43^\circ 34' 37''$ [which introduces a factor $\cos(\Lambda + \frac{\pi}{2})$], $f_b = 68.95 \text{ Hz}$. This value is modified in practice by the backscatter-induced pulling discussed here and by dispersion-induced pushing and can be modified by a transverse magnetic field on the plasma. The scale factor G of this instrument (the ratio of the angular frequency of the interferogram to the normal projection Ω' of the mechanical angular frequency) is therefore 8.62×10^6 . (In gyro jargon this is $G' = 6.65 \text{ counts/arc s}$.)

The granite table in turn is supported by metal pantographs, incorporating worm gear drives (to allow some height and tilt adjustment) and resting on a cubic meter concrete pier, itself bonded with stainless steel rods into the local basalt rock. This system is installed in an underground cavern 30 m below ground level. This gives major benefits for mechanical stability and for temperature stability. The latter is further enhanced in that the room in which the laser is housed ($5 \text{ m} \times 5 \text{ m}$) is thermally in good contact with the cavern. An ancillary room containing much of the peripheral equipment—rf generator, computers, etc.—has more thermal insulation in order to raise the temperature and lower the humidity and give less short-term changes to cavern temperature. Adjustment of the net backscatter phase ζ is most simply achieved by moving weights to flex the Zerodur table and so changing the various partial perimeters z_n , which appear in Eq. (A1). The signal, whether interferometric or single beam, is detected by a photomultiplier and captured on a two-channel Strobes Acquisition PC unit (equivalent to Rapid Systems 360) using CHART software. Processing including FFTs of 8 ksample–128 ksample records is performed using MATLAB 4.2 on a PC 486 and FFTs of records up to 6 million samples on a SUN SparcStation 2000 system.

On the model proposed by Aronowitz [7], the fractional amplitude scattering coefficients may be estimated assuming that a fraction r_β^2 of the intensity of any beam is scattered uniformly at each reflection. In a cavity of

perimeter P and with four mirrors, these reflections occur at a rate of order $4c/P$, and if the scattering is assumed for simplicity to be uniform, a fraction $d\Omega/4\pi$ of this intensity is scattered into the other beam. $d\Omega$ is the acceptance solid angle of that beam and is of the order of $\pi\theta^2$, where θ is the diffraction angle characterizing the beam. $\theta = \lambda/\pi\sigma_0$, σ_0 being the spot size at the waist. Hence the fractional amplitude backscatter rate r_\pm is of order $2r_\beta c\lambda/(\pi P\sigma_0)$ and for the Canterbury ring laser, where we estimate $\sigma_0 \simeq 0.66 \text{ mm}$, one might expect a lock-in threshold $l \sim 10^4 r_\beta \text{ Hz}$. For mirrors with the manufactured values of scatter (of order ppm in intensity), this implies $r_\beta \sim 10^{-3}$ and so lock-in thresholds $l \sim 10 \text{ Hz}$, which is significantly less than the unpulled Sagnac frequency f induced by the Earth's rotation. The laser is thus expected to be unlocked solely by the Sagnac effect of the Earth's rotation.

Pulling effects could therefore be as low as $l/2f^2$ or 1%, even in dissipative coupling. This, however, represents an ideal from which we are presently somewhat removed, basically because of those economies of construction for our laser, which require us to use Viton O-ring seals and prevent a standard clean room environment. Under the conditions in which the data reported here were taken, it is common for the lock-in threshold to be a more substantial fraction of, or even exceed, the Sagnac frequency. In the last case the ring may be unlocked only by choosing the conservative coupling regime. Also for reasons of economy, we have been unable to achieve the full potential of the cavern for temperature stability; some sources of heat from ancillary equipment are yet to be isolated properly and thermal lagging of the fairly extensive passages of the cavern to reduce convective air flows has yet to be installed. Since, as shown below, temperature variation is the principal cause of beat frequency drift at present, it is planned to reduce this by better thermal insulation, reduced heat fluxes, and fuller mechanical decoupling of the Zerodur plate.

Under present conditions, temperature changes cause drift in the pulled frequency of up to several hertz over runs of several hours' duration and cause the average mode frequency to drift at the rate of the order of one megahertz per minute. The latter estimate (drift in the mode frequency) is obtained by a variety of methods. The simplest, but least direct, is to monitor the pulled beat frequency by a JFTA analysis and observe a cyclic pattern as the mirrors shift from thermal expansion and cycle the system (and so the lock-in threshold and the frequency pulling) between the conservative and dissipative regimes. More directly, we have beaten a single output beam (from say the CCW beam) against a Newport NL-1 stabilized laser, which is frequency shifted into near coincidence by an acousto-optic modulator, and detecting the mode shift using a Newport SR-130 supercavity as a Fabry-Pérot analyzer. This reflects both the perimeter change with temperature and the drift in the Newport NL-1 stabilized laser. Third, we have increased power to enter the multimode states and then heterodyned the beats between adjacent longitudinal modes (nominally 86.34 MHz, corrected by their dispersive splittings) against a local rf frequency scanner, and observed

the relative frequency drift. All three methods, but more particularly the first and the third, indicate a common dependence of frequency drift on thermal expansion of the ring.

The drift of the pulled frequency is affected by a total perimeter change because of the consequential changes in dispersion as the modes wander through the gain curve of the He-Ne plasma; this source of drift itself is dealt with by stabilizing the perimeter. Apart from this, the pulled frequency drift is affected equally by any change in mirror separations z_n , through Eq. (A1). Several important consequences follow. Since a factor 2 appears in the exponent of Eq. (A1), when backscatter changes (as opposed to dispersion changes) are the dominant source of drift, a full cycle of change in the drift is achieved when the cavity length is changed by a half (as opposed to a whole) wavelength. In this sense, the effects of backscatter cycle twice as quickly as those of dispersion, given the same temperature-induced changes in physical positions. The dependence of the pulled frequency on backscatter phase can be (and currently is) more important in practice than its dependence on the dispersive effects of changes in mode frequency. When backscatter dominates drift effects, stabilization of the perimeter and so the mode frequency is of very limited value in stabilizing the beat frequency against temperature-induced changes in ring dimensions, since any localized perimeter adjustment of say one mirror position has a different symmetry from the roughly homogeneous effects of temperature, and will not in general aid towards restoring the original net backscatter phase ζ . Rodloff [20] overcame this in a relatively small ring by using more than one piezocontrolled mirror element to permit independent adjustment of several distances z_n contributing to the backscatter phase and so to eliminate changes in ζ . The introduction of any piezoelectric element itself compromises thermal stability and as described above perimeter stabilization through use of a single piezoelectric element is ineffective in reducing pulled beat frequency drifts over time scales of the order of minutes. The topic of this paper, in particular the consideration of alternative schemes of direct stabilization of the backscatter phase using a more relevant diagnostic than the perimeter or the mode frequency, is then of considerable practical importance as well as interest.

In view of the significantly reduced pulling and so enhanced stability achievable in conservative coupling, we suggest as a candidate for this diagnostic the relative phase of the intensity modulations for the counterrotating beams. Servicing any perimeter adjustment, even for a single piezocontrolled mirror element, to maintain the value 180° for this relative phase should ensure a substantial reduction in drift not only because the net backscatter phase ζ is then held constant, but also because at this value (when $\zeta = \pi/2$) pulling effects are minimized. Clearly this scheme will not be helpful in simultaneously stabilizing the perimeter and so many dispersion-related drifts, unless at least one more control is introduced. We may ask whether it suffices to record one beam only with the interferogram and then deduce the phase relationship between the single beams from the information con-

tained in the two records, including their relative phase. The answer is not immediately obvious, since intensity variations in either beam are correlated with their (undetected) phase only through the above theory and the connection involves in principle the difference $\epsilon_+ - \epsilon_-$ of the individual backscatter phases as well as their sum 2ζ . However, within the model of Sec. IID, the temporal phases of the three beams are related [Eq. (C16)] and two-channel detection should suffice to determine and monitor ζ . We have not been able to verify this experimentally and quantitatively at this stage; sometimes the single-beam spectra remain rigidly in antiphase while the interferometer phase varies smoothly with respect to each single beam over wide variations of ζ . This is at least partly because the interferometer phase (relative to either single-beam phase) is a sensitive function of interferometer alignment and partly because of the variation in backscatter magnitude with monotonic thermal dimensional changes.

B. Experimental observations

With this ring laser system, the most sensitive run to date is a week-long run (94AG26; 6.92 d, 19–26 August 1994, 598 122 s, 20 samples per second). Only a single beam intensity was monitored in this run, so that we depended on pulling effects to modulate the beam intensity and reveal the Sagnac fringes. Even so, the signal-to-noise ratio was of the order of 30 dB (contrary to some conventions, we define the decibel level by $10\log_{10} V$ and not $20\log_{10} V$, where V is the raw photomultiplier tube voltage, since the latter is already a measure of intensity and not amplitude). In our initial analysis, the one considered in greatest detail below, the cutoff frequency f_{cut} and Nyquist frequency f_N used in the numerical dedrifting method were 0.0005 Hz and 0.625 Hz, respectively, since we chose every 16th sample in the run. This was so as to give a manageable number ($N = 747\,654$; such numbers are reduced slightly to a power of two times an integer for faster FFTs) of samples for processing. Since the run duration was retained, the frequency resolution capability inherent in its reciprocal, the frequency bin size ($1.6914 \mu\text{Hz}$), was preserved. This gives a Sagnac line from the Earth's rotation that can be fitted by a Gaussian with an accuracy of 140 nHz in the line position (Fig. 1). This frequency accuracy is a factor 8 better than that ($1 \mu\text{Hz}$) given in our last report [1]. The linewidth from this fit gives a full width at half maximum power of $6.2 \mu\text{Hz}$.

The expected rms frequency fluctuation [1] as measured by a full width at half maximum power (FWHMP) has the form

$$\delta f = \sqrt{2hf_0^3 B/Q^2 P_o T}. \quad (41)$$

This ‘‘quantum noise’’ limit has been documented for lasers and compared with $1/f$ noise, etc., on several occasions [26–28]. This width will be affected by a variety of considerations. One curious property of all figures [29,17–19] such as Fig. 1 is that the FWHMP is invariably a small number (say 4) times the frequency bin size $f_{\text{bin}} = 1/T$, which itself changes by more than four or-

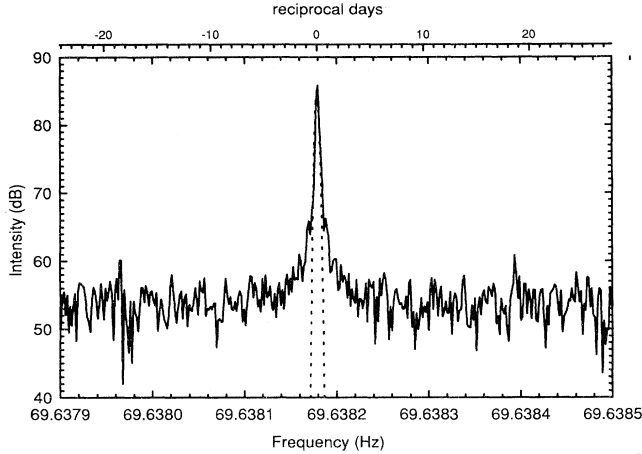


FIG. 1. Sagnac line from Earth rotation for the run 94AG26 (19–26 August 1994), using dedrifting as described in the text.

ders of magnitude in this progression. This reflects in part the tendency to choose a standard value for the file size N , namely, a value that is convenient for processing purposes. The bandwidth B is the Nyquist frequency $N/2T$ (since the electronic bandwidth is much greater) and from Eq. (41) the ratio of FWHMP to bin size is the product of \sqrt{N} and a number that depends only on the laser, not the data sampling rate or length:

$$\frac{\delta f}{f_{\text{bin}}} = \sqrt{\frac{hf_0^3}{Q^2 P_o}} \sqrt{N}. \quad (42)$$

To estimate this number, we need the product $Q^2 P_o$.

The measurement of Q has been based on two different measurement techniques, one involving a ringdown time when radio frequency pumping is turned off and the other involving the asymmetry in the cavity response to a swept frequency [30]. A recent remeasurement of the ringdown time in our ring for this purpose gives $\tau = 25 \pm 1 \mu\text{s}$, where the error is comparable with the simultaneously measured decay time for the plasma glow and hence $Q = 2\pi f_0 \tau = 7.5 \pm 0.3 \times 10^{10}$.

This figure is a new record, as far as we are aware, for the quality factor of an optical device. It demonstrates an improvement in the general performance of the ring over the two years since the previous reported value (4.5×10^{10}) was so obtained, reflecting newer mirrors, improved cleanliness of outgassing, the feasibility now of vacuum bakeout, and the installation of a clean air system. It is still significantly less than the quality factor [$Q_{\text{max}} = 2\pi P/\lambda(1-R^4) = 8.6 \times 10^{11}$], which is commensurate with the mirror specifications at manufacture (total loss per mirror $1-R$ of ≤ 10 ppm), corresponding in fact to a total loss per mirror of 115 ppm, comparable to the loss determined by the manufacturer on mirrors returned by us. The associated finesse F is $\lambda Q/P$, giving $F = 14\,000$ and similarly $F_{\text{max}} = 160\,000$.

We now obtain the total power loss P_o arising from all causes including vignetting, etc., from the measurements

of Q and of output beam power P_t at any port under single-mode operation. We find (at near the limit of our power meter) $P_t = 1.5 \pm 1$ nW. Since $Q = 2\pi f_0 E_c/P_o$, the circulating power $E_c = 2P_t P/cT$, and T is the power transmittance of a mirror (1.2 ± 0.1 ppm in our case) we can estimate the power loss as $P_o = 2P_t P/\tau cT = (1.3 \pm 0.8) \times 10^{-6}$. This gives in Eq. (41) a FWHMP of $4 \pm 3 \mu\text{Hz}$ for the initial choice of sample number ($N \simeq 750\,000$). This is less than the observed value, which therefore is a consequence of other effects. The effect of Nuttall windowing of the data needs detailed analysis and gives a width of the same order as a few bins [29]. Processing much larger files should increase the numerical bandwidth and the quantum noise component of the FWHMP and reveal the shot noise. We have not been able to confirm this; at the limits of our processing ability on a SUN SparcStation 2000 we chose an effective sample rate of 10 samples/s and so $N \simeq 6$ million, for which we might expect via Eq. (42) a FWHMP approximately equal to $13 \mu\text{Hz}$, approximately double the observed FWHMP for the original N value; in fact no appreciable increase of this FWHMP was seen. This is unexpected, even with the errors mentioned. The effect of the dedrifting algorithm on quantum noise also needs fuller analysis to help determine whether our ring quality factor Q is so high that quantum noise as well as $1/f$ noise has been reduced to an insignificant level.

We give in Fig. 2 the instantaneous frequency as a function of time in this data run. The first half of this run has a markedly smaller drift than has previously been reported, reflecting recent improvements to the mechanical isolation of the Zerodur slab and to the thermal stabilisation of the cavern, for example, by moving dehumidifiers outside the control shacks and by installing heat exchangers on the dehumidified air to bring it nearer the cavern temperature before its recirculation. Our mirrors were not optimally clean, however, and the present results are capable of significant improvement. As such, the role of backscatter is significant, even with the present low temperature drifts. This, with many other such results, some of which are given later and some of which involve comparing the observed temperature drifts with the known thermal expansion of the Zerodur block and are not detailed here, indicates that drifts are associated principally with changes in backscatter phase. With the

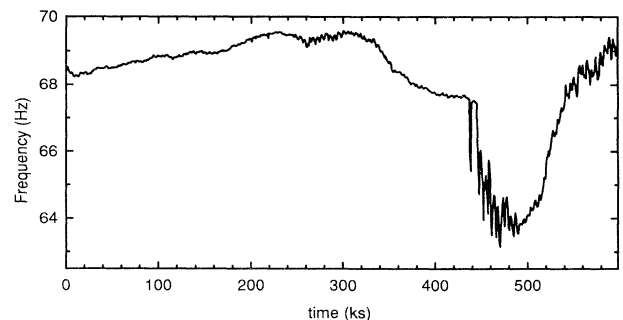


FIG. 2. Instantaneous frequency drift during the run 94AG26 of Fig. 1.

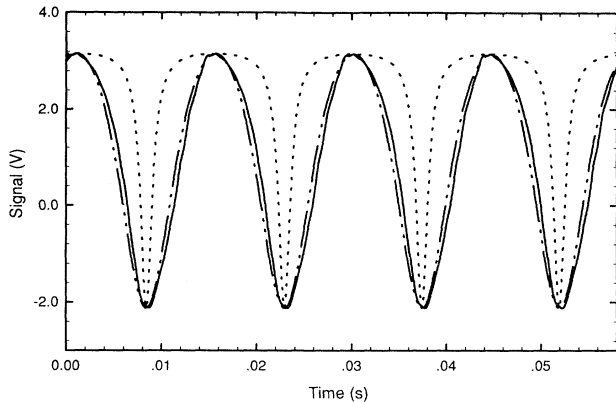


FIG. 3. Temporal wave forms as predicted by Eq. (13) and an experimental measurement of an interferogram (solid line: also used in Figs. 4 and 5) for comparison. The various curves are for $l/f = 0.327$ (dash-dotted) and 0.95 (dotted).

kinds of thermal stabilization currently used, the period of the cycling that is often apparent in the instantaneous frequency between dissipative and conservative coupling and hence changes in mirror separation of the order of a half wavelength can be increased to well over 1 d.

We have verified the theory given in this paper that in many situations and particularly when pulling is not large enough to lock but still dominates the beam dynamics, the wave form of any of the single beam intensity, the interferogram, the instantaneous frequency, however these may be derived, has the form of Eq. (13), which is related to the Airy function [Eq. (17)] and has a geometric progression of harmonics. In Fig. 3 we give a typical result for small pulling and compare it with plots of Eq. (13) for various choices of the parameter, to illustrate this Airy-like behavior. Asymmetric wave forms can be found for moderate to high pulling. The evidence is clearer in the frequency domain. In Fig. 4 we plot the Fourier spectra of the interferogram and of the instantaneous phase

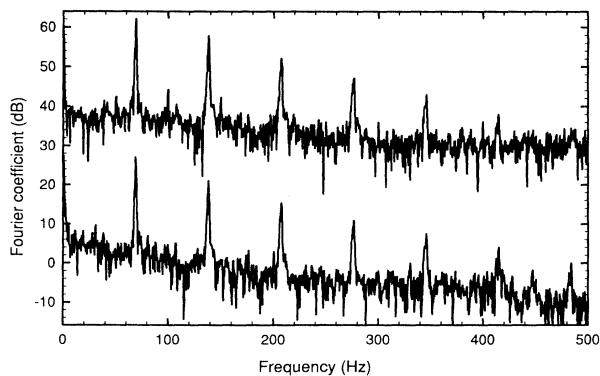


FIG. 4. Harmonic analysis (FFT) of an interferogram (upper curve) and of the instantaneous phase (lower curve) from the run of Fig. 3. Since the peaks in this log-linear plot lie on lines, the harmonic amplitudes form geometric progressions. The ratios of the geometric progressions are indistinguishably close, at $r = 0.34 \pm 0.01$.

derived from it by the analytic signal technique. The validity of a geometric progression is readily tested in such a decibel (log-linear) plot: the peaks should form a straight line. In this example (2048 samples from run G0402S01, taken at 1000 samples per second) the approximation of the geometric progression is satisfactory and ratios r derived from the two signals are 0.34 ± 0.01 for the interferogram and 0.34 ± 0.04 for the instantaneous frequency (for which an ω factor has been included in each harmonic amplitude). Since there is negligible difference between these ratios, we may estimate using the theory given in this paper that the gain parameter a is much greater than the pulled frequency p . The unpulled frequency f is estimated to be 68.97 ± 0.10 Hz from the various harmonic frequencies in the interferogram of Fig. 4 and 69.05 ± 0.12 Hz from the instantaneous phase, so that $h/a \sim 1$. These values for the unpulled frequency are in excellent agreement with the Sagnac value. The ratio for the harmonics of the instantaneous frequency is greater than that for the interferogram, as expected from the above theory, and so uncertainties in extracting the unpulled frequency increase. For example, in run CR3013, a sample of the same length and duration gave $f = 69.8$ Hz, $r_I = 0.060 \pm 0.02$, and $r = 0.26 \pm 0.10$.

For the case of single beam spectra, we have studied a sequence of situations in which the net backscatter phase ζ , as determined by the relative phase of the single beams, is set at several values in the range $0-2\pi$. The change was made by adding weights to the Zerodur table, slightly bending it, and altering the mirror separations. The results are given in Table I, the last decimal place giving the order of the accuracy of each measurement, and plotted in Fig. 5. In Table I the units of ζ are degrees and each ζ value is stable to within 1° during the run ISJA11. Frequency pulling effects follow the trends expected. There is least pulling when the backscatter phase ζ is close to $\pi/2$ (the conservative coupling case) and most when $\zeta = 0, \pi$ (the dissipative case). Harmonic effects only qualitatively follow the trends expected (smallest harmonic ratio r_I and so weakest harmonics in the conservative coupling case). f , p , and l are the unpulled, the pulled, and the threshold lock-in frequency, respectively. As the system moves from the dissipative regime ($\zeta = 0, \pi$) to the conservative ($\zeta = \pi/2$), the pulling is reduced, the pulled frequency rises (again some magnetic biasing was applied to raise f above the nominal Sagnac frequency), and the ratio of harmonics is altered. The

TABLE I. Results for a set of runs (with two-channel single beam detection of 2048 samples at samples/sec) in which the net backscatter phase ζ , as measured by the relative phase of the fluctuations in the counterrotating beam intensities, was set at a variety of values.

p	r_I	f/l	ζ
67.9	0.03	16	12
70.3	0.02	24	50
73.0	0.05	10	95
69.5	0.09	6	142
67.1	0.08	7	177

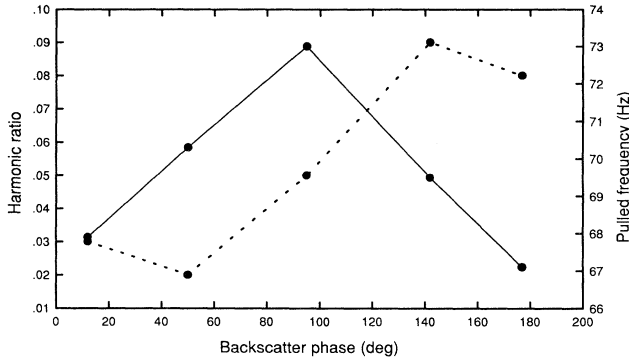


FIG. 5. Comparison of the pulled beat frequency (solid line) and the ratio r for the geometrical progression of harmonics (dotted line) for a series of runs as given in Table I.

discrepancy in the pulled frequencies for $\zeta = 0, \pi$ shows us that the monotonic change of the mirror positions has steered the laser beam onto new mirror spots where the backscatter characteristics are appreciably different and helps to explain why in the bottom rows of the table the ration r does not increase again after the expected (and found) overall decrease in the first rows.

In monitoring the relative phase of CW and CCW beam intensity variations, it is convenient to form a Lissajous pattern from these by x - y plotting on an oscilloscope. The system is attracted to either the conservative case of antiphase intensity variations or the dissipative case of in-phase variations, with a strength that is considerably greater when backscatter is relatively large or when other coupling effects conspire to raise the lock-in threshold. For example, when natural neon is used this strength of attraction increases as the lock-in threshold l approaches the unpulled frequency f , whereas with isotopically enriched neon ($\text{Ne}^{20}:\text{Ne}^{22} \sim 1:1$) it is easier to verify that separating mirrors by up to a quarter of a wavelength takes the relative phase of the two beam intensities smoothly through the range $0-\pi$. We attribute the relative difficulty of the same demonstration for natural neon ($\text{Ne}^{20}:\text{Ne}^{22} \sim 9:1$) to the effective increase in beam coupling of dispersion effects associated with hole burning in the plasma for the natural isotopic mixture. Such a behavior may be expected from the earlier analyses, as described in Sec. IID. This suggests that the analytical solutions given earlier in this paper should therefore cover, at least approximately, a majority of the cases of interest and importance provided isotopically enriched neon is used and that l is not greater than f .

V. CONCLUSIONS

The harmonic structure of the interferogram and of the single beam intensities, while also if approximately of the character of a geometrical progression with the pulled frequency as the fundamental, is in general less rich than that of the instantaneous phase, the amplitude variations taking strength from the higher harmonics. The phase

relationships between these various signals, like the lock-in threshold, is a sensitive function of the net backscatter phase and so of the mirror separations. Removing the associated drift of the pulled frequency requires a different kind of stabilization method to the perimeter stabilization normally used to stabilize a mode in a cavity and could conceivably be performed by comparing the phase of the intensity variations of two such signals so as to maintain conservative coupling and minimal pulling.

ACKNOWLEDGMENTS

We are grateful to Dr. R. Rodloff for discussions. H.R.B. acknowledges partial support from the NSF under the U.S.-New Zealand Cooperative Science Program, and L.Z. and G.E.S. acknowledge support from FRST Contracts Nos. UOC 305 and 408.

APPENDIX A: BACKSCATTERING PHASES

In this appendix we review and extend the analysis of Rodloff [20] for the distance dependence of the net backscatter phase and reinterpret and extend the analysis of Haus *et al.* [5] for the time-reversal constraints on this phase at each scatterer.

Backscattering contributes to the time evolution of each beam's phasor at, say, A . The various backscatter centers around the ring are labeled by n , each being at the optical path length $z_{n\pm}$ from A in the appropriate direction. At the n th center, each phasor \tilde{E}_{\pm} has a distance-induced phase shift relative to A of $\exp(-i\omega_{\pm}z_{n\pm}/c)$. Each wave then scatters off center n with a local amplitude and phase shift defined by a complex backscattering amplitude factor $\tilde{A}_{n\pm}$ to give a phasor $\tilde{A}_{n\pm}\tilde{E}_{\pm}\exp(i\omega_{\pm}t - i\omega_{\pm}z_{n\pm}/c)$. This then propagates back to A , with the effect of adding a further phase factor $\exp(i\omega_{\pm}z_{n\mp})$. Hence the phasor accumulates a distance-dependent phase shift at A of $\exp -i\omega_{\pm}(z_{n\pm} - z_{n\mp} + P_{\mp})/c$. To a very good approximation (of the order of 10^{-5} rad in our system) we may ignore the nonreciprocities in ω_{\pm}, P_{\pm} (and use instead the average values ω, P , respectively) in the phase of this expression, so that for this part of the calculation we may take $z_{n+} \simeq P - z_{n-} \equiv z_n$ and use $\omega P = 2\pi cN$ to show that the return journey doubles the distance-dependent phase [20]; the effect of backscattering at A is then to inject per unit time a complex fraction

$$R_{\mp} = \sum_n \tilde{A}_{n\mp} \exp(2i\omega z_n/c) \quad (\text{A1})$$

of one amplitude \tilde{E}_{\mp} into the other \tilde{E}_{\pm} .

The form of this expression is of fundamental importance. Note first that the distance-dependent phase is identical for both beams; the backscatter fractions R_+, R_- differ only through the difference between $A_{n\pm}$, i.e., the nonreciprocity of local backscattering amplitudes [20]. We define amplitudes and phases of these fractions by $R_{\mp} = r_{\mp} \exp i\epsilon_{\mp}$ and similarly for the local scattering

amplitudes $\tilde{A}_{n\pm} = A_{n\pm} \exp i\epsilon_{n\pm}$. The net phases ϵ_+, ϵ_- are critically dependent not only on the phases $\epsilon_{n\pm}$ of the backscatter at each center but also on the separation z_n between the centers through the common factor $\exp(i2\omega z_n/c)$.

As regards the former dependence, Haus *et al.* [5] showed (ignoring the effects of partial perimeters z_n) that the symmetry and reality (more generally, the Hermiticity) of a response tensor such as the susceptibility or polarizability is sufficient to guarantee conservative coupling at the local level for each scatterer. In the notation used here, the value $\pi/2$ for $2\zeta = \epsilon_{n+} + \epsilon_{n-}$ reflects a Hermitian character for the polarizability tensor linking the applied electric field to derived polarization in the scattering particle n .

This property can be traced further still, as indeed for the Sagnac frequency itself [1], to fundamental constraints arising from time reversal. A more fundamental description of the origin of such Onsager-like symmetries of response tensors is that of time-reversal symmetry. We show and extend this here within a general quantum mechanical formalism. The counterpart in a quantum picture to the susceptibility tensor of Haus *et al.* is the expression

$$\begin{aligned} \chi &= A \sum_{a,b,c} e^{-E_a/kT} \left(\frac{\langle b|V(\mathbf{e})|c\rangle \langle c|V(\mathbf{e}')|a\rangle}{E_a - E_c + \hbar\omega} \right. \\ &\quad \left. + \frac{\langle b|V(\mathbf{e}')|c\rangle \langle c|V(\mathbf{e})|a\rangle}{E_a - E_c - \hbar\omega'} \right) \\ &= \sum_{a,b} e^{-E_a/kT} \langle b|\mathbf{O}|a\rangle, \end{aligned} \quad (\text{A2})$$

where A is a numerical factor, a, b, c are initial, final, and intermediate electronic states, radiation states are suppressed for simplicity, $(\mathbf{e}, \omega), (\mathbf{e}', \omega')$ denote the polarization vector and the frequency of the incoming (absorbed) and the reradiated (emitted) photons in the corresponding virtual interaction process, and k, T are Boltzmann's constant and temperature. The photons are associated with the incident electric field and the induced polarization \mathbf{P} , respectively, and interact with the electronic systems through the coupling Hamiltonian V , which, depending on the choice of gauge, may be written as $-q\mathbf{A}(\mathbf{e}) \cdot \mathbf{p}/m$ or $-q\mathbf{E}(\mathbf{e}) \cdot \mathbf{r}$ [31,32]. In this problem we take initial and final states a, b to be degenerate, so that only Rayleigh scattering is significant: $\omega = \omega'$.

In the case that we apply closure to the intermediate-state-dependent denominators and ignore the photon energies in the denominator (thus assuming that the electronic energy differences, being nonresonant, will be more significant), the effective operator \mathbf{O} satisfies the constraint of being HT symmetric ($\mathbf{O} = \tilde{\mathbf{O}}^\dagger$). This leads to the response-tensor Hermiticity condition required by Haus *et al.* for dissipative coupling, directly from the fundamental property of antilinearity of time reversal $\langle a|V|b\rangle = \langle \bar{a}|\tilde{V}|\bar{b}\rangle^* = \langle \bar{b}|\tilde{V}^\dagger|\bar{a}\rangle$, coupled with the realization that in an otherwise time-even system a ket $|a\rangle$ may be replaced by its time reverse $|\bar{a}\rangle$ in the summations of Eq. (A2) without affecting the thermal or the

energy factors. More details of such arguments are in earlier works [31,32].

APPENDIX B: PHASOR DIAGRAMS FOR CONSERVATIVE AND DISSIPATIVE COUPLING

Physical interpretations of the role of laser gain may be offered in the context of dissipative and of conservative coupling [11]. The counterrotating beams form a standing wave light pattern at rest in the local Lorentz frame, the beat signal being produced as the detector moves past the beads of the necklace [33]. In the absence of backscatter and pulling, the necklace is unaffected by the instantaneous position of the mirrors and detector. However, as has been shown vividly in recent demonstrations [15,16], for the dissipative case backscatter or vignetting has the effect of constraining the movement of the beads of the necklace, which responds as far as is practicable by altering the bead positions so as to minimize losses [5] in such an active device. If an imperfect output mirror is only slowly dragged along the necklace, the beads on the latter are carried along with it; the laser is locked. At faster speeds the laser unlocks and the beads "slip" periodically on the mirrors, thus undoing some of their enforced motion in between the more "frictional" parts of the interaction. The first effect of this is that the necklace is moved in a jerky or sawing motion, thus adding harmonics to the original interferogram and also giving a periodic variation to the instantaneous frequency Eq. (13). Second, the laser beams have to recover lost energy in the interim through laser gain. This makes the intensity of each beam fluctuate accordingly [Eq. (2)]; the difference in this dynamic behavior of the instantaneous frequency (the bead position) and the beam or interferogram intensity (the bead size) is a direct reflection of the importance of laser gain on the time scale of all related effects (the inverse of the pulled frequency).

In the case that $a = \beta = \xi = 0$, Eq. (1) takes the simplified form

$$\frac{d\tilde{E}_\pm}{dt} = i\omega_\pm \tilde{E}_\pm + r_\mp \tilde{E}_\mp \exp i\epsilon_\mp. \quad (\text{B1})$$

A simple perspex model on an overhead projector displays the major predictions (Fig. 6); the phasor diagrams follow those of Wilkinson [11]. Two phasors represent the beam amplitudes and rotate with respect to each other since $\omega_+ - \omega_- \neq 0$. A proportion r_\mp (assumed constant) of one phasor is added to the other, affecting the time dependence of the magnitude and angle of each phasor in a way that is characteristic of the additional phases generated by the backscattering factors $\exp i\epsilon_\mp$ through the sum $\zeta = (\epsilon_+ + \epsilon_-)/2$. If $\zeta = 0 \bmod \pi$, corresponding to a symmetrical pattern of phasor addition [Fig. 6(a)], it is readily perceived from the diagram (or better, from a model) that the phasors have the same length at any instant (i.e., beam intensities are the same function of time), but that their relative angle (frequency pulling) is maximally affected by backscatter. This corresponds to dissipative coupling. If $\zeta = \pi/2 \bmod \pi$, phasor addi-

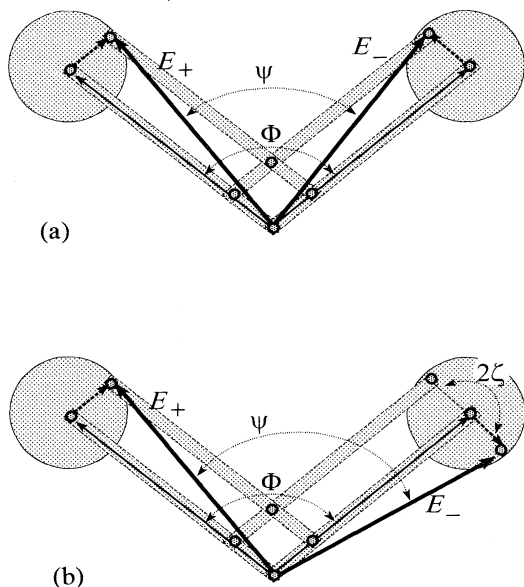


FIG. 6. A simple visualization of the effects of pulling on phasor amplitude and angle. A perspex parallelogram structure (filled areas) smoothly hinged at the small circles permits a proportion (dashed vector) of one beam phasor (thin solid vector) to be added to another, giving the final phasors (thick solid vectors). $\Phi \equiv (\omega_+ - \omega_-)t$ increases in time linearly and is the nominal Sagnac phase; $\psi(t)$ is this phase adjusted for pulling. (a) Dissipative coupling. $\psi(t)$ is alternately smaller and larger than $\Phi(t)$ as the latter varies from 0 to π and from π to 2π , respectively. On average, it is less, hence the frequency is pulled down. (b) Conservative coupling. The geometry ensures that $\psi(t)$ is equal to $\Phi(t)$ and is a linear function of t .

tion has an antisymmetrical character [Fig. 6(b)] and the phasor length variations are in antiphase, while their relative angle is a constant, so that the instantaneous phase shows no pulling effects in the approximations used here. This corresponds to conservative coupling.

APPENDIX C: FULLER NOTES ON DERIVATIONS OF SEC. II

1. Dissipative case

For the dissipative case, we note that an alternative method for deriving ψ is given in connection with the analytic signal approach in Sec. III. Note from Eq. (11) that the limiting case $l \rightarrow 0$ retrieves the linear accumulation of the phase $\psi \rightarrow 2\pi ft$, which corresponds to a signal of constant frequency f . Note also that $f^2 + v^2 = f \sec^2 \pi pt (f + l \sin 2\theta)$, where

$$\theta \equiv \pi pt + \chi/2, \quad (\text{C1})$$

so that

$$\cos \psi = \frac{f^2 - v^2}{f^2 + v^2} = \frac{p \cos 2\theta}{f + l \sin 2\theta}, \quad \tan \psi = \frac{l + f \sin 2\theta}{p \cos 2\theta}. \quad (\text{C2})$$

The moments of the wave form are defined in general by $\bar{f}_0^n \equiv (1/T) \int_0^T f_0^n(t) dt$. The first moment or mean frequency is

$$\bar{f}_0 = \frac{2(f+l)}{\pi} \int_0^{\pi/2} \frac{dx}{(\cos^2 x + u \sin^2 x)} = \frac{f+l}{\sqrt{u}} = p \quad (\text{C3})$$

(see integral 647 in [34] or integral 2.553 in [35]). Similarly,

$$\begin{aligned} \bar{f}_0^2 &= \frac{2(f+l)^2}{\pi} \int_0^{\pi/2} \frac{dx}{(\cos^2 x + u \sin^2 x)^2} \\ &= (f+l)^2 \frac{(u+1)}{2u\sqrt{u}} = fp \end{aligned} \quad (\text{C4})$$

(see integral 648 in [34] or integral 2.553 in [35]). Hence the standard deviation in the pulled frequency is

$$\sigma \equiv \sqrt{\bar{f}_0^2 - \bar{f}_0^2} = \sqrt{p(f-p)} \simeq \frac{l}{\sqrt{2}}. \quad (\text{C5})$$

A Fourier analysis gives

$$\begin{aligned} F_n &= \frac{2}{T} \int_0^T f_0(t) \cos\left(\frac{2\pi nt}{T}\right) dt \\ &= \frac{2(f+l)}{\pi} \int_{-\pi/2}^{\pi/2} \frac{\cos(2nx) dx}{\cos^2 x + u \sin^2 x} \end{aligned} \quad (\text{C6})$$

$$= \frac{2f^2}{\pi} \int_0^\pi \frac{\cos ny dy}{f - l \cos y} = 2pr^n \quad (\text{C7})$$

(see integral 3.613 in [35]).

Equation (14) admits the solution $f = \rho(1+r^2)$, $l = 2\rho r$ for an arbitrary constant ρ . Hence Eq. (13), and by integration Eq. (C2), can be reexpressed as

$$f_0 = \frac{p(1-r^2)}{1+r^2-2r \cos 2\pi pt}, \quad \psi = \arctan\left(\frac{r \sin 2\pi pt}{1+r \cos 2\pi pt}\right), \quad (\text{C8})$$

where the integration constant is subsumed into ψ . This leads to the Airy function as described in the text for the representation of the pulled wave form.

For the case $b = 0$ (in which the effect of pumping a is either weak or, for short times, comparatively unregulated) the solution is

$$E = e^{2\pi at} (f + l \sin 2\theta). \quad (\text{C9})$$

This result, valid for times previous to its runaway behavior becoming inappropriate, clearly displays intensity variations in sympathy with the instantaneous frequency variations and with the same modulation depth. When neither b nor a is zero, Eq. (18) can be linearized and so integrated by making the substitution [14]

$E = \pi a / [b - J \exp(-2\pi a t)]$, which gives the linear differential equation

$$\frac{dJ}{dt} + 2\pi l J \cos \psi = 2\pi b l e^{2\pi a t} \cos \psi. \quad (\text{C10})$$

The integrating factor for Eq. (C10) is $F = \exp(2\pi l \int dt \cos \phi) = f + l \sin(2\pi p t + \chi)$ and so

$$J = \frac{2\pi b l p}{f + l \sin(2\pi p t + \chi)} \left(\int dt \cos 2\theta e^{2\pi a t} + K \right) \quad (\text{C11})$$

$$= \frac{b l p e^{2\pi a t} (p \sin 2\theta + a \cos 2\theta) + 2\pi b l p K / h^2}{h^2 (f + l \sin 2\theta)}, \quad (\text{C12})$$

K being a constant of integration, so that Eq. (19) follows. The last term in the denominator of Eq. (19), not retained by Etrich *et al.*, is needed for compatibility with Eq. (C9), but can be ignored in the long time limit.

Equation (20) led to an argument in which backscatter and beam intensity variations were seen to tend to cancel. This scenario is modified by the harmonic contributions from the $\sin 2\theta$ factor in the numerator of Eq. (19), which are important only when l is a substantial fraction of f . In the general case, we find from inserting the Fourier decomposition of the denominator of Eq. (19) into that equation that up to an overall constant the n th harmonic has the amplitude

$$A_n = -P f r_I^n / 2 + l (r_I^{n+1} - Q r_I^{n-1}), \quad (\text{C13})$$

where P, Q are phase factors dependent on angles such as χ, γ . For low gain or lock in ($h f \gg a l$), the geometric progression has the ratio $r_I \simeq |A_n / A_{n-1}| \rightarrow a l / 2 h f$.

The interferometer wave form [Eq. (22)] has a time dependence that is similar to that of the single beams [Eq. (19)]. Indeed, the denominators of these equations are identical and hence the harmonic structure that they on their own imply is also the same. The numerator however involves a different admixture of dc and fundamental signals, so that the general harmonic amplitude has the form [in analogy to Eq. (C13)]

$$A_n = -P' i r_I^n / 2 + (r_I^{n+1} - Q' r_I^{n-1}), \quad (\text{C14})$$

where again P', Q' are phase factors. Once again, for low gain or lock in, A_n is proportional to r_I^{n+1} so that the harmonics form a geometric progression with ratio $r_I \rightarrow a l / 2 h f$; when *either* l or a tends to zero, r_I also vanishes; harmonic content of the interferogram from a ring laser is contingent on the existence *both* of pulling *and* of laser gain and the relative strengths of the higher

harmonics for the are paradoxically less for the interferogram than for the instantaneous frequency since the intensity fluctuations tend to offset the harmonic effect of the phase fluctuations.

2. General case

In the general case, it is useful to note that the extrema of the beam intensities and of the instantaneous frequency occur at times t_{\pm}, t_F when from Eqs. (33) and (34)

$$\cos(\psi(t_{\pm}) \mp \zeta) = 0, \quad \cos \psi(t_F) = 0, \quad (\text{C15})$$

respectively. Hence the extremal phase value for, say, a maximum of the instantaneous frequency is the numerical average of those for the maxima of the two single beam intensities. In the limit of small backscatter and pulling (when ψ is approximately linear in time, with coefficient $2\pi p$) the extremal time t_F for the instantaneous frequency fluctuations also is the average of the corresponding times t_{\pm} for the two single beams. The separation in time immediately gives the relative phase ζ

$$|t_+ - t_F| = |t_- - t_F| = \zeta / 2\pi p. \quad (\text{C16})$$

For stronger pulling, the nonlinearity in the dependence of ψ on time will complicate these mutual phase relationships, which will be defined by the solution of Eq. (C15) together with Eq. (35) for the extremal times. Since this nonlinear behavior gives the result [Eq. (12), with the redefinitions of this section] that the instantaneous frequency spends the majority of its time below its median value, the separations between the extremal times may be expected to be less than those given by Eq. (C16). We note that even in this nonlinear case, all beams as well as the interferogram have their phases adjusted by the phase difference $\epsilon_+ - \epsilon_-$ in such a way (*viz.*, entirely through the quantity ψ) that the respective times at which the intensities of the counterrotating beams reach their respective extremal values depend on the backscattering phases only through ζ .

It may be noted also that a Fourier analysis of $F(t) \equiv \tan \psi$ gives a geometric progression similar to Eq. (C7): $\Gamma_{2\pi n p} = \Gamma_{2\pi p} r_F^n$, where (again from integral 3.613 in [35]) $r_F = -R(1/r)$. For small r , $r_F = -r/2$; the tangent of the instantaneous phase is more harmonic than the raw signals. As r tends to 1, r_F tends to -1 : substantial anharmonicity is shared by both kinds of spectra. However, the relationship between these ratios is nonlinear.

-
- [1] G. E. Stedman, M. T. Johansson, Z. Li, C. H. Rowe, and H. R. Bilger, *Opt. Lett.* **20**, 324 (1995).
 [2] J. Zhang, T. Feng, S. Zhang, and G. Jin, *Appl. Opt.* **31**, 6459 (1992).
 [3] A. Kapitulnik, J. S. Dodge, and M. M. Fejer, *J. Appl.*

- Phys.* **75**, 6872 (1994).
 [4] H.-J. Weber, A. Burau, and J. Blechschmidt, *Phys. Rev. B* **49**, 6991 (1994).
 [5] H. Haus, H. Statz, and I. W. Smith, *IEEE J. Quantum Electron.* **QE-21**, 78 (1985).

- [6] R. Adler, reprinted in *Proc. IEEE* **61**, 1380 (1973).
- [7] F. Aronowitz, in *Laser Applications*, edited by M. Ross (Academic, New York, 1971), Vol. 1, pp. 133–200.
- [8] F. Aronowitz and R. J. Collins, *J. Appl. Phys.* **41**, 130 (1970).
- [9] W. W. Chow, J. Gea-Banacloche, L. M. Pedrotti, V. E. Sanders, W. Schleich, and M. O. Scully, *Rev. Mod. Phys.* **57**, 61 (1985).
- [10] H. Statz, T. A. Dorschner, M. Holtz, and I. W. Smith, *Laser Handbook*, edited by M. L. Stitch and M. Bass (North-Holland, Amsterdam 1985), Vol. 4, pp. 229–332.
- [11] J. R. Wilkinson, *Prog. Quantum Electron.* **11**, 1 (1987).
- [12] W. R. Christian and L. Mandel, *Phys. Rev. A* **34**, 3932 (1986).
- [13] W. R. Christian and L. Mandel, *J. Opt. Soc. Am. B* **7**, 1406 (1988).
- [14] C. Etrich, P. Mandel, R. Centeno Neelen, R. J. C. Spreeuw, and J. P. Woerdman, *Phys. Rev. A* **46**, 525 (1992).
- [15] F. Bretenaker, B. Lepine, A. Le Calvez, O. Adam, J.-P. Taché, and A. Le Floch, *Phys. Rev. A* **47**, 543 (1993).
- [16] F. Bretenaker, J.-P. Taché, and A. Le Floch, *Electron. Lett.* **21**, 291 (1993).
- [17] G. E. Stedman, H. R. Bilger, Li Ziyuan, M. P. Poulton, C. H. Rowe, I. Vetharanim, and P. V. Wells, *Aust. J. Phys.* **46**, 87 (1993).
- [18] H. R. Bilger, G. E. Stedman, M. P. Poulton, C. H. Rowe, Ziyuan Li, and P. V. Wells, in *Ring Laser for Precision Measurement of Non-reciprocal Phenomena*, special issue of *IEEE Trans. Instrum. Meas.* **42**, 407 (1993); *IEEE Trans. Instrum. Meas.* **43**, 102(E) (1994).
- [19] R. Anderson, H. R. Bilger, and G. E. Stedman, *Am. J. Phys.* **62**, 975 (1994).
- [20] R. Rodloff, *IEEE J. Quantum Electron.* **QE-23**, 438 (1987), Eq. 12a.
- [21] H. R. Bilger, Z. Li, and G. E. Stedman, *Appl. Opt.* (to be published).
- [22] H. R. Bilger, G. E. Stedman, Ziyuan Li, U. Schreiber, and M. Schneider, in *Ring Lasers for Geodesy*, special issue of *IEEE Trans. Instrum. Meas.* (April 1995).
- [23] A. V. Oppenheim and R. W. Schäfer, *Discrete-Time Signal Processing* (Prentice-Hall, Englewood Cliffs, 1989).
- [24] L. R. Rabiner and B. Gold, *Theory and Application of Digital Signal Processing* (Prentice-Hall, Englewood Cliffs, 1975).
- [25] R. Rodloff, *Z. Flugwiss. Weltraumforsch.* **18**, 2 (1994).
- [26] T. A. Dorschner, H. A. Haus, I. M. Holz, I. W. Smith, and H. Statz, *IEEE J. Quantum Electron.* **QE-16**, 1376 (1980).
- [27] M. R. Sayeh and H. R. Bilger, *Phys. Rev. Lett.* **55**, 700 (1985).
- [28] H. R. Bilger and M. R. Sayeh, in *Noise in Physical Systems and 1/f Noise*, edited by A. D'Amico and P. Mazzetti (Elsevier, Amsterdam, 1986), pp. 293–296.
- [29] G. E. Stedman and H. R. Bilger, *Digital Signal Processing* **2**, 105 (1992).
- [30] Li Ziyuan, R. G. T. Bennett, and G. E. Stedman, *Opt. Commun.* **86**, 51 (1991).
- [31] G. E. Stedman, *Diagram Techniques in Group Theory* (Cambridge University Press, Cambridge, England, 1990), Chap. 7.
- [32] G. E. Stedman, in *Modern Nonlinear Optics Part II: Advances in Chemical Physics Series*, edited by S. Kielich and M. W. Evans (Wiley, New York, 1993), Vol. 85, pp. 489–544.
- [33] E. O. Schulz-Dubois, *IEEE J. Quantum Electron.* **QE-23**, 299 (1987).
- [34] *CRC Handbook of Mathematical Sciences*, edited by W.H. Beyer, 6th ed. (CRC, Boca Raton, FL, 1987).
- [35] I. S. Gradshteyn and I. M. Ryzhik, *Tables of Integrals, Series and Products*, 4th ed. (Academic, New York, 1980).